

# **Supporting Information:**

## **How does bending the uranyl unit influence its spectroscopy and luminescence**

Hanna Oher,<sup>†</sup> André Severo Pereira Gomes,<sup>‡</sup> Richard E. Wilson,<sup>\*,¶</sup> David D. Schnaars,<sup>¶</sup> and Valérie Vallet<sup>\*,‡</sup>

<sup>†</sup>*Univ Rennes, CNRS, ISCR (Institut des Sciences Chimiques de Rennes) – UMR 6226,  
F-35000 Rennes, France*

<sup>‡</sup>*Univ. Lille, CNRS, UMR 8523 - PhLAM - Physique des Lasers Atomes et Molécules,  
F-59000 Lille, France*

<sup>\*</sup>*Chemical Sciences and Engineering Division, Argonne National Laboratory, Lemont,  
Illinois 60439, United States*

E-mail: rewilson@anl.gov; valerie.vallet@univ-lille.fr

## List of Tables

S1	Symmetric ( $\nu_s$ ) and asymmetric ( $\nu_{as}$ ) vibrational modes of the uranyl ions (cm $^{-1}$ ), bond length (Å) and angles (°) for UO <sub>2</sub> Cl <sub>2</sub> (phen) <sub>2</sub> optimized at the DFT-PBE0-D3 level of theory in the gas-phase and in a CPCM water solvent.	S-4
S2	$\Delta E$ (in kJ mol $^{-1}$ ) electronic energy difference between the linear and bent structures optimized at the DFT-PBE0-D3 level of theory, computed with different XC functionals.	S-5
S3	Binding energies $\Delta E$ (in kJ mol $^{-1}$ ) to the UO <sub>2</sub> Cl <sub>2</sub> complex of the phen ligand in axial or equatorial position, computed at the PBE0-D3 level of theory.	S-6
S4	Natural population analysis of the uranium 6d and 5f orbitals, taken as the difference to the U <sup>VI</sup> oxidation state; atomic charges; QTAIM characteristics in atomic units of the U ≡ O, U–Cl, and U–N <sub>ax</sub> , U–N <sub>eq</sub> Bond Critical Points, and QTAIM delocalization indices $\delta(U-L)$ ; Wiberg bond orders WBO(U – L) in UO <sub>2</sub> Cl <sub>2</sub> (Phen) <sub>2</sub> PBE0-D3 gas-phase structures with bent and linear conformations.	S-7
S5	SR-ZORA-TDDFT (CAM-B3LYP) vertical transition energies (in cm $^{-1}$ ) in linear and bent UO <sub>2</sub> <sup>2+</sup> computed at the UO <sub>2</sub> Cl <sub>2</sub> (phen) <sub>2</sub> PBE0-D3 geometries.	S-8
S6	SR-ZORA-TDDFT (CAM-B3LYP) vertical transition energies (in cm $^{-1}$ ) in UO <sub>2</sub> Cl <sub>4</sub> <sup>2-</sup> computed at the Cs <sub>2</sub> UO <sub>2</sub> Cl <sub>4</sub> geometry. <sup>S1</sup>	S-9
S7	SR-ZORA-TDDFT (CAM-B3LYP) vertical transition energies (in cm $^{-1}$ ) in UO <sub>2</sub> Cl <sub>2</sub> computed at the gas-phase PBE0-D3 geometry.	S-9
S8	Vertical transition energies (in cm $^{-1}$ ) computed at the spin-orbit level (SO-ZORA) (CAM-B3LYP) for in UO <sub>2</sub> Cl <sub>2</sub> (TDDFT and TDA approximation), and UO <sub>2</sub> Cl <sub>2</sub> Ar <sub>2</sub> (TDDFT), all computed at the optimized gas-phase PBE0-D3 geometries.	S-9

S9	SR-ZORA-TDDFT (CAM-B3LYP) vertical transition energies (in $\text{cm}^{-1}$ ) in $\text{UO}_2\text{Cl}_2(\text{phen})_2$ computed at PBE0-D3 gas-phase geometry in the gas-phase and in the COSMO solvent. . . . .	S-10
S10	Assignments of the $\text{UO}_2\text{Cl}_2$ and $\text{UO}_2\text{Cl}_2(\text{phen})_2$ theoretical luminescence spectra computed in the gas phase. The energies of the spectra were adjusted to the theoretical vertical emission energy of the first electron transition. . . . .	S-11
S11	Assignment of the $\text{UO}_2\text{Cl}_4^{2-}$ theoretical luminescence spectrum (taken from Table S4 in Ref. S2). The energy of the spectrum was adjusted to the experimental band-origin value of $\text{Cs}_2\text{UO}_2\text{Cl}_4$ complex. . . . .	S-12

## List of Figures

S1	FT-IR spectrum of crystals of $\text{UO}_2\text{Cl}_2(\text{phen})_2$ in KBr after isotope exchange of the terminal oxo-units of the uranyl. . . . .	S-13
S2	Raman spectrum of crystals of $\text{UO}_2\text{Cl}_2(\text{phen})_2$ after isotope exchange of the terminal oxo-units of the uranyl. . . . .	S-14

Note that the data (input/output) corresponding to the QC calculations of this paper are available at the Zenodo repository.<sup>S3</sup>

## 1 Justification for performing all the calculations in the gas phase

We detail here the reasons justifying that all calculations have been performed in the gas phase. The first reason is to be consistent with experimental data, as we aim at comparing single crystal data to our theoretical calculations. A solid medium may be represented by a dielectric medium of infinite permittivity, which cannot be set in the two quantum chemistry programs we used, namely Gaussian 16<sup>S4</sup> and ADF.<sup>S5</sup> However, to quantify long-range effects, we have optimized the geometry of  $\text{UO}_2\text{Cl}_2(\text{phen})_2$  immersed in a water solvent with  $\varepsilon_r = 80$  described by the continuum polarizable conductor model (CPCM).<sup>S6,S7</sup> The obtained geometries and frequencies are reported in Table S1 together with the gas-phase values. We can note that long-range solvent effects change by few hundreds of Å the uranium-ligand bond distances and by at most  $21 \text{ cm}^{-1}$  the internal uranyl stretching frequencies, thus making calculations in the gas-phase fully suitable.

Table S1: Symmetric ( $\nu_s$ ) and asymmetric ( $\nu_{as}$ ) vibrational modes of the uranyl ions ( $\text{cm}^{-1}$ ), bond length (Å) and angles (°) for  $\text{UO}_2\text{Cl}_2(\text{phen})_2$  optimized at the DFT-PBE0-D3 level of theory in the gas-phase and in a CPCM water solvent.

XC func	Method	$\nu_s$	$\nu_{as}$	$\text{U}\equiv\text{O}$	$\text{O}\equiv\text{U}\equiv\text{O}$	$\text{U}-\text{Cl}$	$\text{U}-\text{N}_{\text{ax}}$	$\text{U}-\text{N}_{\text{eq}}$
PBE0	GP	898	961	1.753	163.4	2.662	2.816	2.699
PBE0-D3	GP	896	957	1.754	162.7	2.660	2.789	2.680
PBE0-D3	CPCM	891	936	1.754	163.3	2.697	2.794	2.648

The comparison of transition energies computed at the scalar relativistic level in the gas-phase and with a conductor-like screening model (COSMO)<sup>S8–S10</sup> for the water solvent reported in Table S9 further illustrates that long-range interactions have a negligible effects on excitation energies, shifting them up by at most  $474 \text{ cm}^{-1}$ .

## 2 Comparison of several exchange-correlation functionals on the uranyl bending energy of $\text{UO}_2\text{Cl}_2(\text{phen})_2$

In Table S2, we compare the bending energy  $\Delta E$  of the  $\text{UO}_2\text{Cl}_2(\text{phen})_2$  complex as computed with several exchange correlation (XC) functionals, such as PBE,<sup>S11</sup> generalized gradient approximation (GGA), several hybrids PBE0,<sup>S11,S12</sup> B3LYP,<sup>S13–S15</sup> BHLYP<sup>S16</sup> with varying amounts of Hartree-Fock Exchange, two range-separated functionals, CAM-B3LYP<sup>S17</sup> and HSE06<sup>S18</sup> and two methods with exact Hartree-Fock exchange, M06HF.<sup>S19,S20</sup>

Table S2:  $\Delta E$  (in  $\text{kJ mol}^{-1}$ ) electronic energy difference between the linear and bent structures optimized at the DFT-PBE0-D3 level of theory, computed with different XC functionals.

Functional	Type	$\Delta E$
PBE	GGA	26.6
B3LYP	Hybrid	20.6
BHLYP	Hybrid	15.9
PBE0	Hybrid	22.0
PBE0+D3	Hybrid + D3	25.3
CAM-B3LYP	RSE	21.0
HSE06	RSE	22.5
M06HF	eX	27.6
HF	eX	4.4

<sup>a</sup> Type refers to the placement of the given functional into the hierarchy of density functional approximations outlined in Ref. S21: generalized gradient approximation (GGA), hybrid, range-separated (SE), exact exchange (eX).

## 3 Binding energy of phen ligands in $\text{UO}_2\text{Cl}_2(\text{phen})_2$

The binding energies of axial and equatorial phen ligands to the  $\text{UO}_2\text{Cl}_2$  complex are reported in Table S3.

Table S3: Binding energies  $\Delta E$  (in  $\text{kJ mol}^{-1}$ ) to the  $\text{UO}_2\text{Cl}_2$  complex of the phen ligand in axial or equatorial position, computed at the PBE0-D3 level of theory.

Reaction	$\Delta E$
$\text{UO}_2\text{Cl}_2 + \text{phen} \longrightarrow \text{UO}_2\text{Cl}_2(\text{phen})_{\text{ax}}$	-167.5
$\text{UO}_2\text{Cl}_2 + \text{phen} \longrightarrow \text{UO}_2\text{Cl}_2(\text{phen})_{\text{eq}}$	-250.2

## 4 QTAIM and NBO analysis

Table S4: Natural population analysis of the uranium 6d and 5f orbitals, taken as the difference to the U<sup>VI</sup> oxidation state; atomic charges; QTAIM characteristics in atomic units of the U≡O, U–Cl, and U–N<sub>ax</sub>, U–N<sub>eq</sub> Bond Critical Points, and QTAIM delocalization indices  $\delta(U-L)$ ; Wiberg bond orders WBO(U–L) in UO<sub>2</sub>Cl<sub>2</sub>(Phen)<sub>2</sub> PBE0-D3 gas-phase structures with bent and linear conformations.

Bond	$\rho_b$	$\nabla^2 \rho_b$	$H_b$	$ V /G$	$\delta(U, L)$	WBO(U – L)
bent–UO <sub>2</sub> Cl <sub>2</sub> (phen) <sub>2</sub>						
U≡O	0.32	0.28	−0.31	1.81	1.91	2.07
U–Cl	0.07	0.14	−0.01	1.28	0.59	0.92
U–N <sub>ax</sub>	0.03	0.09	0.00	1.09	0.20	0.28
U–N <sub>eq</sub>	0.04	0.11	0.00	1.11	0.24	0.30
n(d)	1.68					
n(f)	2.67					
q(U)	1.22					
q(O <sub>yl</sub> )	−0.53					
q(Cl)	−0.41					
q(N <sub>ax</sub> )	−0.35					
q(N <sub>eq</sub> )	−0.38					
linear–UO <sub>2</sub> Cl <sub>2</sub> (phen) <sub>2</sub>						
U≡O	0.33	0.27	−0.32	1.83	1.92	2.05
U–Cl	0.07	0.14	−0.02	1.29	0.61	0.92
U–N <sub>ax</sub>	0.02	0.06	0.00	1.00	0.12	0.19
U–N <sub>eq</sub>	0.04	0.12	0.00	1.12	0.26	0.30
n(d)	1.65					
n(f)	2.65					
q(U)	1.32					
q(O <sub>yl</sub> )	−0.51					
q(Cl)	−0.41					
q(N <sub>ax</sub> )	−0.36					
q(N <sub>eq</sub> )	−0.40					

## 5 Supplementary tables

Table S5: SR-ZORA-TDDFT (CAM-B3LYP) vertical transition energies (in  $\text{cm}^{-1}$ ) in linear and bent  $\text{UO}_2^{2+}$  computed at the  $\text{UO}_2\text{Cl}_2(\text{phen})_2$  PBE0-D3 geometries.

linear $\text{UO}_2^{2+}$			bent $\text{UO}_2^{2+}$		
State	Conf.	$\Delta E$	State	Conf.	$\Delta E$
$^3\sigma_u\phi$		17 676	$^3\sigma_u\phi$		16 983
			$^3\sigma_u\phi$		17 066
$^3\sigma_u\delta$		19 110	$^3\sigma_u\delta$		18 726
			$^3\sigma_u\delta$		18 734
$^1\sigma_u\phi$		22 555	$^1\sigma_u\phi$		21 640
			$^1\sigma_u\phi$		21 726
$^1\sigma_u\delta$		27 812	$^1\sigma_u\delta \times 2$		27 171
$^3\pi_u\phi$		31 545	$^3\pi_u\phi$		30 173
			$^3\pi_u\phi$		30 252
$^3\pi_u\phi$		31 696	$^3\pi_u\phi$		30 676
			$^3\pi_u\phi$		30 757
$^1\pi_u\phi$		33 898	$^1\pi_u\phi$		32 682
			$^1\pi_u\phi$		32 691
$^3\pi_u\delta$		35 539	$^3\pi_u\delta$		33 373
			$^3\pi_u\delta$		33 459

Table S6: SR-ZORA-TDDFT (CAM-B3LYP) vertical transition energies (in  $\text{cm}^{-1}$ ) in  $\text{UO}_2\text{Cl}_4^{2-}$  computed at the  $\text{Cs}_2\text{UO}_2\text{Cl}_4$  geometry.<sup>S1</sup>

Trans.	$\Delta E$
Tripl. $\sigma_u(51\%) + \text{Cl}(47\%) \rightarrow \delta$	21 985
Tripl. $\sigma_u(48\%) + \text{Cl}(47\%) \rightarrow \delta$	22 810
Tripl. $\sigma_u(45\%) + \text{Cl}(52\%) \rightarrow \phi$	25 079
Tripl. $\sigma_u(45\%) + \text{Cl}(52\%) \rightarrow \phi$	25 292
Sing. $\sigma_u(38\%) + \text{Cl}(59\%) \rightarrow \phi$	29 006
Sing. $\sigma_u(37\%) + \text{Cl}(58\%) \rightarrow \phi$	29 186
Sing. $\sigma_u(34\%) + \text{Cl}(61\%) \rightarrow \delta$	30 024
Sing. $\sigma_u(33\%) + \text{Cl}(57\%) \rightarrow \delta$	30 744

Table S7: SR-ZORA-TDDFT (CAM-B3LYP) vertical transition energies (in  $\text{cm}^{-1}$ ) in  $\text{UO}_2\text{Cl}_2$  computed at the gas-phase PBE0-D3 geometry.

Trans.	$\Delta E$
Trip. $\sigma_u(42\%) + \text{Cl}(57\%) \rightarrow \delta$	20 170
Trip. $\sigma_u(38\%) + \text{Cl}(61\%) \rightarrow \delta$	20 863
Trip. $\sigma_u(34\%) + \text{Cl}(63\%) \rightarrow \phi$	21 223
Trip. $\sigma_u(34\%) + \text{Cl}(63\%) \rightarrow \phi$	21 506
Sing. $\sigma_u(22\%) + \text{Cl}(76\%) \rightarrow \phi$	24 250
Sing. $\sigma_u(22\%) + \text{Cl}(76\%) \rightarrow \phi$	24 610
Sing. $\sigma_u(16\%) + \text{Cl}(82\%) \rightarrow \delta$	26 618
Sing. $\sigma_u(17\%) + \text{Cl}(76\%) \rightarrow \delta$	27 630

Table S8: Vertical transition energies (in  $\text{cm}^{-1}$ ) computed at the spin-orbit level (SO-ZORA) (CAM-B3LYP) for in  $\text{UO}_2\text{Cl}_2$  (TDDFT and TDA approximation), and  $\text{UO}_2\text{Cl}_2\text{Ar}_2$  (TDDFT), all computed at the optimized gas-phase PBE0-D3 geometries.

Trans.	$\text{UO}_2\text{Cl}_2$		$\text{UO}_2\text{Cl}_2\text{Ar}_2$	
	$\Delta E$		$\Delta E$	
	TDDFT	TDA	TDDFT	TDDFT
$\sigma_u(32\%) + \text{Cl}(62\%) \rightarrow \phi(87\%) + \delta(9\%)$	17 303	17 703	17 714	
$\sigma_u(31\%) + \text{Cl}(63\%) \rightarrow \phi(93\%) + \delta(3\%)$	17 466	17 845	17 916	
$\sigma_u(35\%) + \text{Cl}(59\%) \rightarrow \delta(77\%) + \phi(18\%)$	17 979	18 478	18 243	
$\sigma_u(33\%) + \text{Cl}(58\%) \rightarrow \delta(77\%) + \phi(18\%)$	17 990	18 513	18 256	
$\sigma_u(28\%) + \text{Cl}(63\%) \rightarrow \phi(62\%) + \delta(29\%)$	18 374	18 820	18 787	
$\sigma_u(29\%) + \text{Cl}(64\%) \rightarrow \phi(71\%) + \delta(19\%)$	18 475	18 897	18 938	
$\sigma_u(33\%) + \text{Cl}(59\%) \rightarrow \delta(69\%) + \phi(7\%)$	19 814	20 374	20 161	
$\sigma_u(30\%) + \text{Cl}(63\%) \rightarrow \delta(77\%) + \delta(2\%)$	20 159	20 760	20 398	

Table S9: SR-ZORA-TDDFT (CAM-B3LYP) vertical transition energies (in  $\text{cm}^{-1}$ ) in  $\text{UO}_2\text{Cl}_2(\text{phen})_2$  computed at PBE0-D3 gas-phase geometry in the gas-phase and in the COSMO solvent.

	TDDFT/GP	TDDFT/COSMO	
Trans.	$\Delta E$	Trans.	$\Delta E$
Trip. $\pi_{(phen)_{ax}}(57\%) + \text{Cl}(11\%) \rightarrow \pi_{(phen)_{ax}}^*$	21 978	Trip. $\sigma_u(40\%) + \pi_{(phen)_{ax}}(31\%) + \text{Cl}(22\%) \rightarrow \delta$	22 178
Trip. $\sigma_u(36\%) + \pi_{(phen)_{ax}}(23\%) + \text{Cl}(22\%) \rightarrow \delta$	21 989	Trip. $\pi_{(phen)_{ax}}(86\%) + \text{Cl}(10\%) \rightarrow \pi_{(phen)_{ax}}^*$	22 406
Trip. $\pi_{(phen)_{eq}} \rightarrow \pi_{(phen)_{eq}}^*$	22 362	Trip. $\pi_{(phen)_{eq}} \rightarrow \pi_{(phen)_{eq}}^*$	22 665
Trip. $\sigma_u(38\%) + \pi_{(phen)_{ax}}(26\%) + \text{Cl}(23\%) \rightarrow \delta$	22 933	Trip. $\sigma_u(39\%) + \pi_{(phen)_{ax}}(32\%) + \text{Cl}(22\%) \rightarrow \delta$	23 159
Trip. $\sigma_u(36\%) + \pi_{(phen)_{ax}}(25\%) + \text{Cl}(27\%) \rightarrow \phi$	23 635	Trip. $\sigma_u(39\%) + \pi_{(phen)_{ax}}(34\%) + \text{Cl}(24\%) \rightarrow \phi$	24 015
Trip. $\sigma_u(27\%) + \pi_{(phen)_{ax}}(18\%) + \text{Cl}(20\%) \rightarrow \phi + \pi_{(phen)_{ax}}^*$	24 175	Trip. $\sigma_u(38\%) + \pi_{(phen)_{ax}}(31\%) + \text{Cl}(24\%) \rightarrow \phi$	24 460
Sing. $\sigma_u(30\%) + \pi_{(phen)_{ax}}(24\%) + \text{Cl}(34\%) \rightarrow \phi$	27 439	Sing. $\sigma_u(33\%) + \pi_{(phen)_{ax}}(35\%) + \text{Cl}(27\%) \rightarrow \phi$	27 913
Sing. $\sigma_u(22\%) + \pi_{(phen)_{ax}}(18\%) + \text{Cl}(24\%) \rightarrow \phi + \pi_{(phen)_{ax}}^*$	28 051	Trip. $\pi_{(phen)_{eq}} \rightarrow \pi_{(phen)_{eq}}^*$	28 060

Table S10: Assignments of the  $\text{UO}_2\text{Cl}_2$  and  $\text{UO}_2\text{Cl}_2(\text{phen})_2$  theoretical luminescence spectra computed in the gas phase. The energies of the spectra were adjusted to the theoretical vertical emission energy of the first electron transition.

UO <sub>2</sub> Cl <sub>2</sub>			
$E$ [cm <sup>-1</sup> ]	$\Delta E$ [cm <sup>-1</sup> ]	$I$ [au]	Identification
16 529		$5.23 \times 10^{-1}$	$0'(0) \rightarrow 1(0)$
16 476	52	$1.73 \times 10^{-1}$	$0'(0) \rightarrow 1(1\nu_0)$
16 310	219	$5.67 \times 10^{-2}$	$0'(0) \rightarrow 1(1\nu_3)$
16 257	271	$1.45 \times 10^{-2}$	$0'(0) \rightarrow 1(1\nu_0, 1\nu_3)$
16 186	343	$2.15 \times 10^{-3}$	$0'(0) \rightarrow 1(1\nu_6)$
15 579	949	$1.22 \times 10^{-1}$	$0'(0) \rightarrow 1(1\nu_7)$
15 527	52	$3.84 \times 10^{-2}$	$0'(0) \rightarrow 1(1\nu_0, 1\nu_7)$
15 361	219	$9.77 \times 10^{-3}$	$0'(0) \rightarrow 1(1\nu_3, 1\nu_7)$
15 308	271	$2.24 \times 10^{-3}$	$0'(0) \rightarrow 1(1\nu_0, 1\nu_3, 1\nu_7)$
14 630	949	$1.92 \times 10^{-2}$	$0'(0) \rightarrow 1(2\nu_7)$
14 577	52	$5.84 \times 10^{-3}$	$0'(0) \rightarrow 1(1\nu_0, 2\nu_7)$
13 681	949	$2.44 \times 10^{-3}$	$0'(0) \rightarrow 1(3\nu_7)$

$\nu_0$ - Cl-U-Cl scissoring, $\nu_3$ - O <sub>yl</sub> -U-O <sub>yl</sub> bending ,
$\nu_6$ - O <sub>yl</sub> -U-O <sub>yl</sub> bending + U-Cl stretching
$\nu_7$ - symmetrical O <sub>yl</sub> -U-O <sub>yl</sub> stretching

UO <sub>2</sub> Cl <sub>2</sub> (phen) <sub>2</sub>			
$E$ [cm <sup>-1</sup> ]	$\Delta E$ [cm <sup>-1</sup> ]	$I$ [au]	Identification
18 464		$3.75 \times 10^{-1}$	$0'(0) \rightarrow 1(0)$
18 380	84	$1.83 \times 10^{-1}$	$0'(0) \rightarrow 1(1\nu_6)$
18 337	127	$2.94 \times 10^{-2}$	$0'(0) \rightarrow 1(1\nu_{10})$
18 216	248	$1.55 \times 10^{-2}$	$0'(0) \rightarrow 1(1\nu_{21})$
18 183	281	$2.05 \times 10^{-3}$	$0'(0) \rightarrow 1(1\nu_{26})$
17 569	895	$1.10 \times 10^{-1}$	$0'(0) \rightarrow 1(1\nu_{65})$
17 485	84	$5.40 \times 10^{-2}$	$0'(0) \rightarrow 1(1\nu_6, 1\nu_{65})$
17 442	127	$7.45 \times 10^{-3}$	$0'(0) \rightarrow 1(1\nu_{10}, 1\nu_{65})$
17 320	248	$5.95 \times 10^{-3}$	$0'(0) \rightarrow 1(1\nu_{21}, 1\nu_{65})$
16 673	896	$2.13 \times 10^{-2}$	$0'(0) \rightarrow 1(2\nu_{65})$
16 589	84	$1.05 \times 10^{-2}$	$0'(0) \rightarrow 1(1\nu_6, 2\nu_{65})$
16 546	127	$1.28 \times 10^{-3}$	$0'(0) \rightarrow 1(1\nu_{10}, 2\nu_{65})$
16 425	248	$1.37 \times 10^{-3}$	$0'(0) \rightarrow 1(1\nu_{21}, 2\nu_{65})$
15 777	895	$3.29 \times 10^{-3}$	$0'(0) \rightarrow 1(3\nu_{65})$

$\nu_6, \nu_{10}$ - O <sub>yl</sub> -U-O <sub>yl</sub> bending + U-phen stretching ,
$\nu_{21}$ - Cl-U-Cl stretching , $\nu_{26}$ - O <sub>yl</sub> -U-O <sub>yl</sub> + U-phen bending,
$\nu_{65}$ - symmetrical O <sub>yl</sub> -U-O <sub>yl</sub> stretching

Table S11: Assignment of the  $\text{UO}_2\text{Cl}_4^{2-}$  theoretical luminescence spectrum (taken from Table S4 in Ref. S2). The energy of the spectrum was adjusted to the experimental band-origin value of  $\text{Cs}_2\text{UO}_2\text{Cl}_4$  complex.

E [cm <sup>-1</sup> ]	$\Delta\nu$ [cm <sup>-1</sup> ]	I [a.u.]	Identification
19 155		$6.50 \times 10^{-1}$	0'(0)->1(0)
18 918	237.1	$1.43 \times 10^{-2}$	0'(0)->1(1 $\nu_{11}$ )
18 761	394.4	$1.72 \times 10^{-3}$	0'(0)->1(2 $\nu_7$ )
18 261	474.2	$3.29 \times 10^{-4}$	0'(0)->1(2 $\nu_{11}$ )
18 024	894.4	$2.46 \times 10^{-1}$	0'(0)->1(1 $\nu_{14}$ )
18 024	237.1	$7.21 \times 10^{-3}$	0'(0)->1(1 $\nu_{11}$ , 1 $\nu_{14}$ )
17 866	394.4	$6.52 \times 10^{-4}$	0'(0)->1(2 $\nu_7$ , 1 $\nu_{14}$ )
17 786	475.0	$1.84 \times 10^{-4}$	0'(0)->1(2 $\nu_{11}$ , 1 $\nu_{14}$ )
17 366	894.4	$5.91 \times 10^{-2}$	0'(0)->1(2 $\nu_{14}$ )
17 129	237.1	$2.11 \times 10^{-3}$	0'(0)->1(1 $\nu_{11}$ , 2 $\nu_{14}$ )
16 972	394.4	$1.56 \times 10^{-4}$	0'(0)->1(2 $\nu_7$ , 2 $\nu_{14}$ )
16 891	475.0	$5.94 \times 10^{-5}$	0'(0)->1(2 $\nu_{11}$ , 2 $\nu_{14}$ )
16 472	894.4	$1.11 \times 10^{-2}$	0'(0)->1(3 $\nu_{14}$ )
16 235	237.1	$4.66 \times 10^{-4}$	0'(0)->1(1 $\nu_{11}$ , 3 $\nu_{14}$ )
16 077	394.4	$2.95 \times 10^{-5}$	0'(0)->1(2 $\nu_7$ , 3 $\nu_{14}$ )
15 997	475.0	$1.44 \times 10^{-5}$	0'(0)->1(2 $\nu_{11}$ , 3 $\nu_{14}$ )
15 577	894.4	$1.80 \times 10^{-3}$	0'(0)->1(4 $\nu_{14}$ )

$\nu_7$  - O<sub>yl</sub>-U-O<sub>yl</sub> rocking,  $\nu_{11}$  - symmetrical Cl-U-Cl stretching ,  
 $\nu_{14}$  - symmetrical O<sub>yl</sub>-U-O<sub>yl</sub> stretching

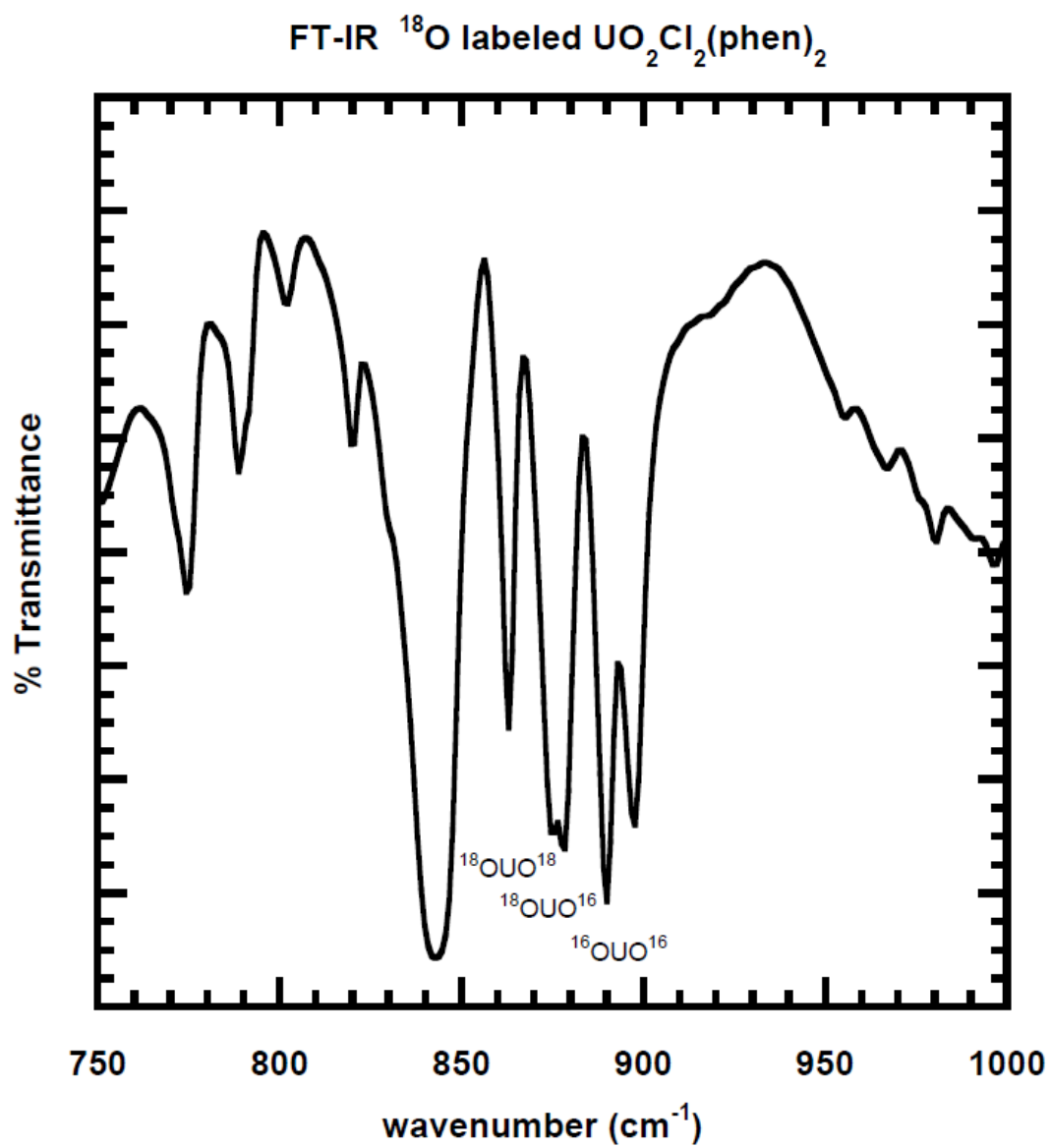


Figure S1: FT-IR spectrum of crystals of  $\text{UO}_2\text{Cl}_2(\text{phen})_2$  in KBr after isotope exchange of the terminal oxo-units of the uranyl.

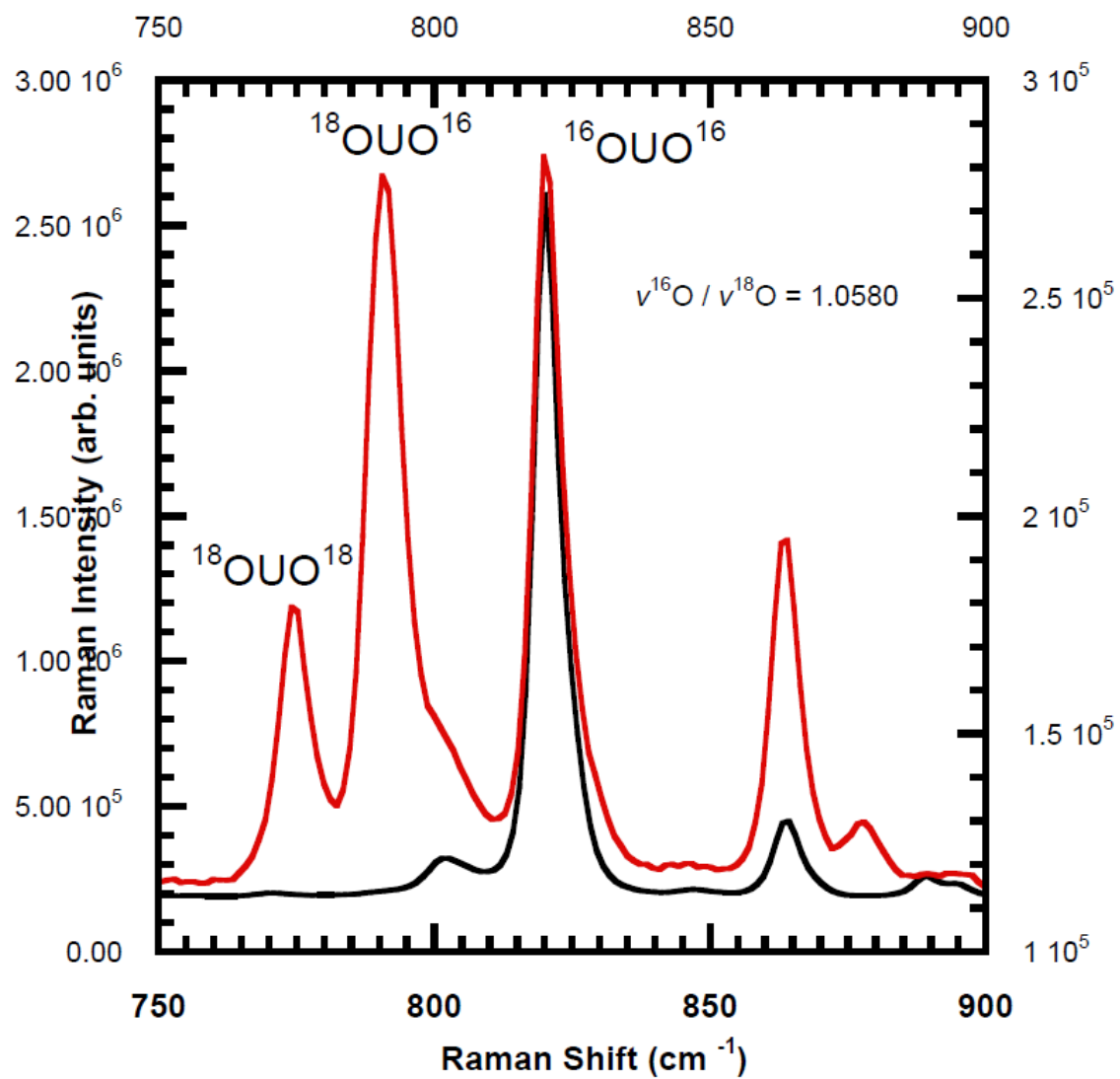


Figure S2: Raman spectrum of crystals of  $\text{UO}_2\text{Cl}_2(\text{phen})_2$  after isotope exchange of the terminal oxo-units of the uranyl.

## References

- (S1) Schnaars, D. D.; Wilson, R. E. Structural and vibrational properties of U(VI) $O_2Cl_4^{2-}$  and Pu(VI) $O_2Cl_4^{2-}$  Complexes. *Inorg. Chem.* **2013**, *52*, 14138–14147, DOI: [10.1021/ic401991n](https://doi.org/10.1021/ic401991n).
- (S2) Oher, H.; Réal, F.; Vercouter, T.; Vallet, V. Investigation of the Luminescence of  $[UO_2X_4]^{2-}$  ( $X = Cl, Br$ ) Complexes in the Organic Phase Using Time-Resolved Laser-Induced Fluorescence Spectroscopy and Quantum Chemical Simulations. *Inorg. Chem.* **2020**, *59*, 5896–5906, DOI: [10.1021/acs.inorgchem.9b03614](https://doi.org/10.1021/acs.inorgchem.9b03614).
- (S3) Oher, H.; Gomes, A. S. P.; Wilson, R. E.; Schnaars, D.; Vallet, V. Dataset: How does bending the uranyl unit influence its spectroscopy and luminescence. DOI: [10.5281/zenodo.7702590](https://doi.org/10.5281/zenodo.7702590).
- (S4) Frisch, M. J.; Trucks, G. W.; Schlegel, H. B.; Scuseria, G. E.; Robb, M. A.; Cheeseman, J. R.; Scalmani, G.; Barone, V.; Petersson, G. A.; Nakatsuji, H.; Li, X.; Caricato, M.; Marenich, A. V.; Bloino, J.; Janesko, B. G.; Gomperts, R.; Mennucci, B.; Hratchian, H. P.; Ortiz, J. V.; Izmaylov, A. F.; Sonnenberg, J. L.; Williams-Young, D.; Ding, F.; Lipparini, F.; Egidi, F.; Goings, J.; Peng, B.; Petrone, A.; Henderson, T.; Ranasinghe, D.; Zakrzewski, V. G.; Gao, J.; Rega, N.; Zheng, G.; Liang, W.; Hada, M.; Ehara, M.; Toyota, K.; Fukuda, R.; Hasegawa, J.; Ishida, M.; Nakajima, T.; Honda, Y.; Kitao, O.; Nakai, H.; Vreven, T.; Throssell, K.; Montgomery, J. A., Jr.; Peralta, J. E.; Ogliaro, F.; Bearpark, M. J.; Heyd, J. J.; Brothers, E. N.; Kudin, K. N.; Staroverov, V. N.; Keith, T. A.; Kobayashi, R.; Normand, J.; Raghavachari, K.; Rendell, A. P.; Burant, J. C.; Iyengar, S. S.; Tomasi, J.; Cossi, M.; Millam, J. M.; Klene, M.; Adamo, C.; Cammi, R.; Ochterski, J. W.; Martin, R. L.; Morokuma, K.; Farkas, O.; Foresman, J. B.; Fox, D. J. Gaussian~16 Revision C.01. 2016; Gaussian Inc. Wallingford CT.

- (S5) ADF2021.106. <http://www.scm.com>.
- (S6) Barone, V.; Cossi, M. Quantum calculation of molecular energies and energy gradients in solution by a conductor solvent model. *J. Phys. Chem. A* **1998**, *102*, 1995–2001, DOI: [10.1021/jp9716997](https://doi.org/10.1021/jp9716997).
- (S7) Cossi, M.; Rega, N.; Scalmani, G.; Barone, V. Energies, structures, and electronic properties of molecules in solution with the C-PCM solvation model. *J. Comput. Chem.* **2003**, *24*, 669–681, DOI: [10.1002/jcc.10189](https://doi.org/10.1002/jcc.10189).
- (S8) Klamt, A.; Schüürmann, G. COSMO: A new approach to dielectric screening in solvents with explicit expressions for the screening energy and its gradient. *J. Chem. Soc. Perkin Trans. 2* **1993**, 799–805, DOI: [10.1039/P29930000799](https://doi.org/10.1039/P29930000799).
- (S9) Klamt, A. Conductor-like screening model for real solvents: a new approach to the quantitative calculation of solvation phenomena. *J. Phys. Chem.* **1995**, *99*, 2224–2235, DOI: [10.1021/j100007a062](https://doi.org/10.1021/j100007a062).
- (S10) Klamt, A.; Jonas, V. Treatment of the outlying charge in continuum solvation models. *J. Chem. Phys.* **1996**, *105*, 9972–9981, DOI: [10.1063/1.472829](https://doi.org/10.1063/1.472829).
- (S11) Perdew, J. P.; Burke, K.; Ernzerhof, M. Generalized gradient approximation made simple. *Phys. Rev. Lett.* **1996**, *77*, 3865–3868, DOI: [10.1103/PhysRevLett.77.3865](https://doi.org/10.1103/PhysRevLett.77.3865).
- (S12) Adamo, C.; Barone, V. Toward reliable density functional methods without adjustable parameters: The PBE0 model. *J. Chem. Phys.* **1999**, *110*, 6158–6170, DOI: [10.1063/1.478522](https://doi.org/10.1063/1.478522).
- (S13) Becke, A. D. Density-functional thermochemistry. III. The role of exact exchange. *J. Chem. Phys.* **1993**, *98*, 5648, DOI: [10.1063/1.464913](https://doi.org/10.1063/1.464913).
- (S14) Lee, C.; Yang, W.; Parr, R. G. Development of the Colle-Salvetti correlation-energy

formula into a functional of the electron density. *Phys. Rev. B* **1988**, *37*, 785–789, DOI: 10.1103/PhysRevB.37.785.

- (S15) Vosko, S. H.; Wilk, L.; Nusair, M. Accurate spin-dependent electron liquid correlation energies for local spin-density calculations - A critical analysis. *Can. J. Phys.* **1980**, *58*, 1200–1211, DOI: 10.1139/p80-159.
- (S16) Becke, A. D. Density-functional thermochemistry. III. The role of exact exchange. *J. Chem. Phys.* **1993**, *98*, 5648–5652, DOI: 10.1063/1.464913.
- (S17) Yanai, T.; Tew, D. P.; Handy, N. C. A new hybrid exchange-correlation functional using the Coulomb-attenuating method (CAM-B3LYP). *Chem. Phys. Lett.* **2004**, *393*, 51–57, DOI: 10.1016/j.cplett.2004.06.011.
- (S18) Krukau, A. V.; Vydrov, O. A.; Izmaylov, A. F.; Scuseria, G. E. Influence of the exchange screening parameter on the performance of screened hybrid functionals. *J. Chem. Phys.* **2006**, *125*, 224106, DOI: 10.1063/1.2404663.
- (S19) Zhao, Y.; Truhlar, D. G. Comparative DFT Study of van der Waals Complexes: Rare-Gas Dimers, Alkaline-Earth Dimers, Zinc Dimer, and Zinc-Rare-Gas Dimers. *J. Phys. Chem. A* **2006**, *110*, 5121–5129, DOI: 10.1021/jp060231d.
- (S20) Zhao, Y.; Truhlar, D. G. Density Functional for Spectroscopy: No Long-Range Self-Interaction Error, Good Performance for Rydberg and Charge-Transfer States, and Better Performance on Average than B3LYP for Ground States. *J. Phys. Chem. A* **2006**, *110*, 13126–13130, DOI: 10.1021/jp066479k.
- (S21) Perdew, J. P.; Schmidt, K. Jacob's ladder of density functional approximations for the exchange-correlation energy. *AIP Conf. Proc.* **2001**, *577*, 1–20, DOI: 10.1063/1.1390175.